Protonium formation in the $\bar{p}$-H collision at low energies by a diabatic approach

M. Hesse,* A. T. Le, and C. D. Lin
Department of Physics, Cardwell Hall, Kansas State University, Manhattan, Kansas 66506, USA
(Received 3 November 2003; published 14 May 2004)

We present a diabatization technique in combination with the recently developed hyperspherical close coupling (HSCC) method. In contrast to the strict diabatization, our simple diabatization procedure transforms *only* sharp avoided crossings in the adiabatic hyperspherical potential curves into real crossings. With this approach, the weak collision channels can be removed from the close-coupling calculations. This method is used to study the antiproton-hydrogen collision at low energies. In the case of a scaled down (anti)proton mass, we show that a 10-channel calculation is enough to obtain converged cross sections at low energies. The results also indicate that protonium formation occurs mostly to the lowest states of the different excited protonium manifolds.

DOI: 10.1103/PhysRevA.69.052712 PACS number(s): 34.90.+q, 36.10.−k, 31.50.Gh, 31.15.Ja

I. INTRODUCTION

Recently the production and detection of cold antihydrogen atoms has been reported by the ATHENA [1] and the ATRAP [2,3] Collaborations. These experiments represent a very important milestone for the antiproton decelerator (AD) at CERN. As a massive negatively charged particle, the antiproton can form exotic systems by replacing an electron in an atom [4–7]. As an antiparticle, it is a basic ingredient to produce antiatoms. The simplest one, the antihydrogen, can be produced and studied in laboratories [8]. The antihydrogen is important in order to compare matter and antimatter properties and interactions [9,10]. The antiproton can also combine with a proton to form protonium, which is the simplest hadronic form of neutral matter. In particular, it is also of interest to determine the rate of annihilation of the antiproton with the proton [11].

We are here interested in the collision of an antiproton with atomic hydrogen, which can produce protonium in excited states. It has been shown by previous studies [11–14] that protonium formation is important only at low energies, i.e., below the ionization threshold. In particular, we are interested in very low energy collisions where the antiprotons come from cold traps at a temperature of about 4.2 K or less. For such collisions, a full quantum mechanical calculation is desired. However, a full quantum mechanical coupled-channel calculation for this collision system is difficult since the protonium is produced in highly excited states. If we assume the kinetic energy of the antiproton is nearly zero, the protonium will be formed mainly in states with a principal quantum number given by $n=\sqrt{\mu_{p\bar{p}}}\approx 30$, where $\mu_{p\bar{p}}$ is the reduced mass of protonium. That means that a full quantum mechanical calculation would include about 500 channels (from the ground state to $n=30$ excited states of protonium and the entrance channel). For this reason, most of previous approaches [11,12,14] have focused on the total protonium formation cross section, or the formation to different manifolds, but not the formation to specific individual protonium states which are needed if the properties of protonium are to be studied. Recently, Esry and Sadeghpour [15] calculated the formation cross sections to the different protonium states, in cases where the proton mass was scaled down to below 20 a.u. The protonium formation then occurs mostly to the $n=2$ or $n=3$ manifold. In this case, they used about 30 channels to perform the calculation.

A full coupled-channel calculation for $\bar{p}$-H collision is complicated from a practical point of view even if calculations including a few hundred channels are possible. For low energy collisions, it is expected in general that only a few channels are important if proper basis set can be identified. Experience drawn from ion-atom collisions with highly charged ions and the model calculation of Esry and Sadeghpour [15] indicated that only a few dominant channels are populated in such collisions. Clearly it is desirable to use only these dominant channels in the coupled channel calculation. However, the adiabatic potential curves used in the coupled channel calculation usually have numerous avoided crossings which make channel elimination difficult.

Recently we have developed a hyperspherical close-coupling method for studying collisions involving three particles. The method has been applied to a number of ion-atom collision systems [16–19]. For collisions involving multiply charged ions where electron is captured to the excited states, we have tested the channel elimination method. To eliminate channels, we first have to find a simple method to obtain diabatic potential curves. We do not define diabatic potentials in the strict sense such that there are no nonadiabatic couplings after diabatization. Rather we chose to diabatize channels among them where the avoided crossings are very narrow. The weak channels that do not couple strongly with the entrance channel are then eliminated in the coupled channel calculation. The method has been tested by comparing the results from the full calculation and from the truncated calculation to justify the procedure.

In this paper, we will use the hyperspherical close coupling method to the $\bar{p}$-H collision. In order to be able to test the channel truncation method adequately and to study the nature of the channel functions, we will first assume that the

*Present address: Physique Quantique, CP165/82, Université Libre de Bruxelles, B-1050 Brussels, Belgium.

proton mass is equal to 100 a.u. such that the protonium will be formed mostly at $n=7$ excited states at low energies. For a full coupled channel calculation, this would require only about 50 channels which can be easily carried out. Our goal here is to illustrate the diabatization and the channel truncation methods, to identify the nature of those channels that should be kept in the truncated calculation and to confirm that indeed the truncated calculation is adequate for the dominant channels. This test would allow us to select the dominant channels which should be included when the real $\bar{p}$-H collision is calculated and where full calculation with all the channels included is difficult to employ.

This paper is organized as follows. In Sec. II we describe the diabatization technique used in this paper in combination with the hyperspherical close-coupling method. The results for the $\bar{p}$-H collision at low energies with proton mass of 100 a.u. are presented in Sec. III. The last section contains a summary and conclusions.

Atomic units are used throughout the paper unless otherwise indicated.

II. THE DIABATIC HYPERSPHERICAL CLOSE-COUPLING METHOD

The hyperspherical close-coupling method (HSCC) has been used previously to study charge transfer in ion-atom collisions [16–19]. We refer the reader to [16] for details on the method. In this paper we combine HSCC method with a diabatization technique, which transforms the sharp avoided crossings in the adiabatic potential curves into real crossings. The idea is to remove, after the diabatization, weak collision channels from the close-coupling calculations.

Adiabatic and diabatic representations are related by a unitary transformation

$$\Phi^D = C\Phi^A, \tag{1}$$

where Φ^A and Φ^D are adiabatic and diabatic channel functions, respectively, and C is the unitary transformation matrix. It is well known [20,21] that if the transformation matrix is chosen as the solution of the linear equation

$$CP + \frac{dC}{dR} = 0, \tag{2}$$

where the matrix P is given by

$$P_{ij} = -\left\langle \Phi_i^A \left| \frac{d}{dR} \right| \Phi_j^A \right\rangle, \tag{3}$$

then in the diabatic representation all the nonadiabatic coupling terms will vanish. This full diabatic procedure has two drawbacks. First the matrix elements P_{ij} have to be calculated accurately over the whole range of R which is difficult to do especially in the avoided crossing region. Second, the resulting diabatic curves often deviate too much from the adiabatic potential curves such that the simplicity of the adiabatic picture can get lost. Over the years there have been many attempts to find quasi-diabatic representations or to find diabatic Hamiltonian [22–26] such that the resulting potential curves can have real crossings instead of the sharp avoided crossings. Most of these methods require the P-matrix as input which can be calculated accurately in the avoided crossing region only if adiabatic states are calculated over a very densely distributed mesh of points. The alternative method of defining diabatic Hamiltonian is not easy to implement either, and the method would depend critically on the nature of the problem. In the HSCC method as presented in [16], we adopted the smooth/slow-variable discretization (SVD) technique of Tolstikhin *et al.* [27]. In this approach the nonadiabatic coupling matrix P is not calculated as these couplings are implicitly included in the overlap matrix between the channel functions. Within the same spirit, our goal is to perform diabatization using only the overlap matrix elements.

In order to solve this problem and avoid the calculation of nonadiabatic couplings, we choose to approximate the derivative with respect to the hyperradius in Eq. (2) by simple difference. The P_{ij} matrix elements are then given by

$$P_{ij} \approx \frac{1}{\Delta R}(\langle \Phi_i^A(R)|\Phi_j^A(R)\rangle - \langle \Phi_i^A(R)|\Phi_j^A(R+\Delta R)\rangle) \tag{4}$$

and become proportional to the difference of two overlaps of adiabatic functions at two neighboring points. Similarly, the derivative of the C matrix with respect to hyperradius is replaced by

$$\frac{dC_{ij}}{dR} \approx \frac{C_{ij}(R+\Delta R) - C_{ij}(R)}{\Delta R}. \tag{5}$$

By substituting these approximations into Eq. (2), we get a simple equation for the C matrix

$$C_{ij}(R+\Delta R) \approx \sum_k C_{ik}(R)\langle \Phi_k^A(R)|\Phi_j^A(R+\Delta R)\rangle. \tag{6}$$

The C matrix at $R+\Delta R$ is then given by the product of the C matrix at R with the overlaps of adiabatic functions at points R and $R+\Delta R$.

Note that the summation in Eq. (6) runs over all channels. This is required to diabatize all the adiabatic potential curves over the whole space of the adiabatic basis set. However, our goal is to diabatize only the sharp avoided crossings, where usually a small number of channels contributes. Thus we want to limit the summation to these channels. To choose the channels that are really involved in the avoided crossing we notice that the characteristic feature near the sharp avoided crossing is the drastic change of the adiabatic channel functions. Since a measure of the change of the functions is the overlaps, a natural criterion should be based on their magnitude. More specifically, we choose to include in the summation in Eq. (6) only those channels k whose overlaps at two neighboring points satisfy

$$|\langle \Phi_k^A(R_{n+1})|\Phi_j^A(R_n)\rangle| > \alpha. \tag{7}$$

The smaller the parameter α, the more diabatic the final potential curves. The diabatization procedure starts at large distances, where we choose the initial condition for C to be equal to the identity matrix. This means that at large dis-

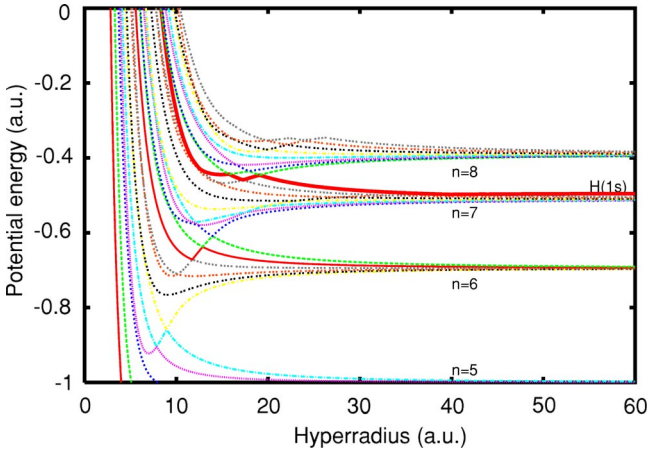

FIG. 1. (Color online) Hyperspherical *adiabatic* potential curves ($J=0$) for $\bar{p}$-H collisions. Only protonium manifolds $n=5,6,7$ and 8 are shown together with the entrance channel which dissociates to H($1s$) and $\bar{p}$.

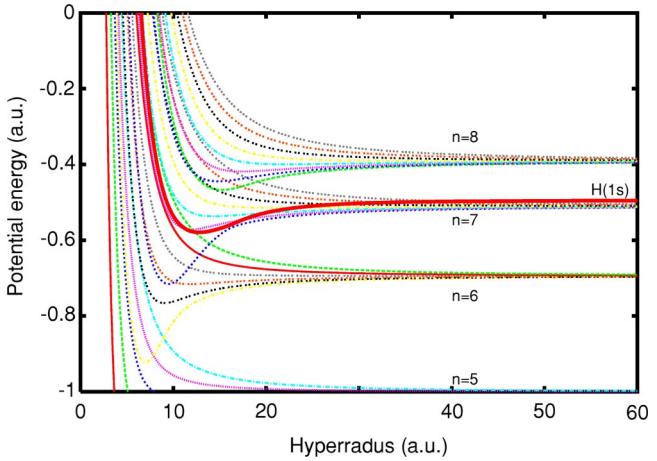

FIG. 2. (Color online) Hyperspherical *diabatic* potential curves ($J=0$) for $\bar{p}$-H collisions. Only protonium manifolds $n=5,6,7$ and 8 are shown together with the entrance channel which dissociates to H($1s$) and $\bar{p}$.

tances, adiabatic and diabatic representations are identical. We then rewrite Eq. (6) as

$$C_{ij}(R_n) \approx \sum_k C_{ik}(R_{n+1})\langle \Phi_k^A(R_{n+1})|\Phi_j^A(R_n)\rangle, \tag{8}$$

where the summation over k is limited by Eq. (7). This equation is used to propagate the C matrix down to $R=0$. Once the diabatic basis is obtained, further implementation of diabatic HSCC is straightforward with the adiabatic channel functions being replaced by the diabatic ones. In practice, we vary α and the step size ΔR_n to make sure that the final cross sections are stable. Typically, we used α equal to 0.2. This diabatization technique has the advantage of providing potential curves not too different from the adiabatic ones (only sharp avoided crossings are transformed). Therefore, our intuitive adiabatic picture of the collision dynamics, based on the important broad avoided crossings, is still valid. Moreover, it is clear that we do not need to calculate the nonadiabatic couplings within this approach.

III. $\bar{p}$-H COLLISION AT LOW ENERGIES

To represent the three-body system formed by the antiproton, the proton and the electron, we choose the Jacobi coordinates defined as follows: the first Jacobi vector $\boldsymbol{\rho}_1$ goes from the antiproton to the electron, and the second vector $\boldsymbol{\rho}_2$ goes from the center of mass of the antiproton-electron pair to the proton. The hyperradius is then given by

$$R = \sqrt{\frac{\mu_1}{\mu}\rho_1^2 + \frac{\mu_2}{\mu}\rho_2^2}, \tag{9}$$

where μ_1 is the reduced mass between the antiproton and the electron, μ_2 is the reduced mass between the proton and the antiproton-electron pair, and μ is an arbitrary mass factor chosen here equal to μ_1.

Figures 1 and 2 represent the adiabatic and diabatic potential curves, respectively, in the case of a proton mass of 100 a.u. and total angular momentum $J=0$. The potential curves are plotted with respect to the hyperradius R at relatively small distances in order to illustrate the region where they interact mostly. Only the protonium states corresponding to the $n=5,6,7$ and 8 manifolds are shown, as they are the closest ones to the H($1s$) entrance channel. The adiabatic potential curves were obtained by solving adiabatic equation in the (θ,ϕ) angular plane, where θ is the angle between the two Jacobi vectors and ϕ is the hyperangle with $\tan\phi = \sqrt{\mu_2/\mu_1}\rho_2/\rho_1$ (see [16]). The diabatic curves were obtained from the adiabatic ones, using the procedure described in the previous section. We denote the protonium states as $|n,j\rangle$, where n represents the manifold, and j gives the position in the manifold ($j \leqslant n$) in the asymptotic region, counting from the lowest one.

From the comparison of these two figures, it is clear that it is easier to identify the different potential curves down to small distances in the diabatic picture. In particular the H($1s$) entrance channel becomes a smooth curve as the sharp avoided crossings occurring between 20 a.u. and 60 a.u. have been transformed into real crossings. One particular avoided crossing between the H($1s$) channel and the $|7,1\rangle$ protonium channel near $R=18$ a.u. has not been diabatized, because it corresponds to a broad avoided crossing. We expect this avoided crossing to play an important role in the protonium formation, leading to the formation of the protonium $|7,1\rangle$ state.

Figure 3 displays the different protonium channel functions at a fixed hyperradius of 100 a.u. At this large distance, diabatic and adiabatic channel functions are identical. The figure shows density contour plots in the (θ,ϕ) angular space. In these plots the range of ϕ is limited to 0.3 radians as the protonium channel functions are localized around the protonium singularity of the Coulomb potential. This singularity occurs at $\theta=\pi$ and $\phi \approx 0.07$. Nodal lines appear in the protonium functions as they correspond to excited states. Belonging to the $n=7$ manifold, these channel functions have the same number of nodal lines. The repartition of nodal curves between the two orientations changes progressively from the lowest state $|7,1\rangle$ to the highest state $|7,7\rangle$.

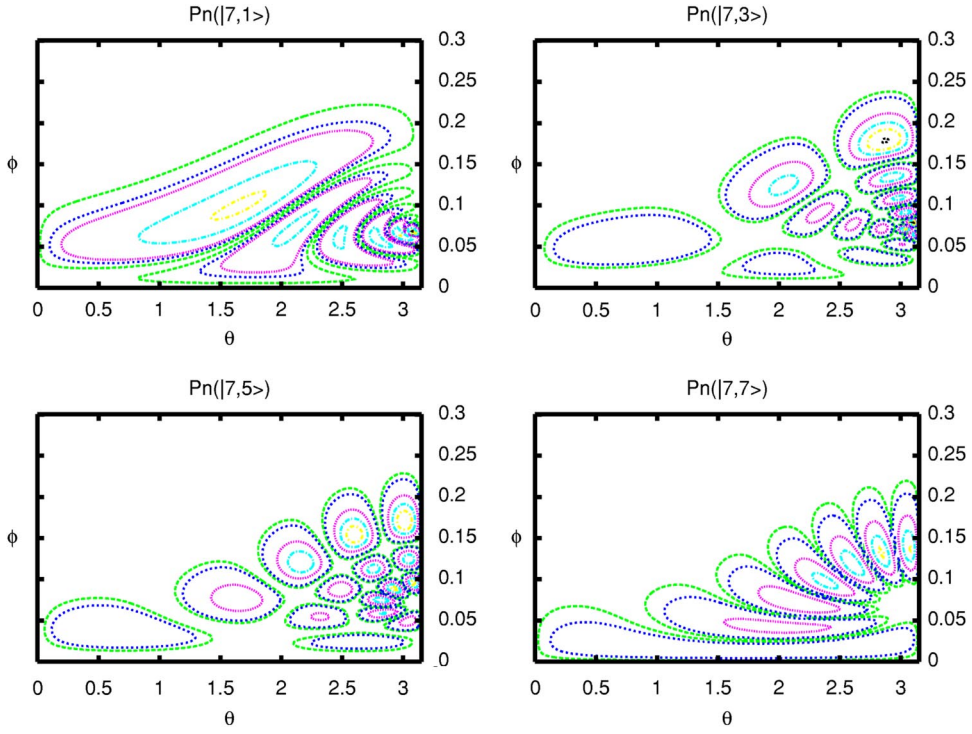

FIG. 3. (Color online) Diabatic channel functions of selective protonium states represented in the (θ,ϕ) angular plane. The protonium states are the $|7,1\rangle$, $|7,3\rangle$, $|7,5\rangle$ and $|7,7\rangle$ states of the $n=7$ manifold. The hyperradius is fixed at 100 a.u.

Figure 4 illustrates the evolution of channel functions with respect to the hyperradius. The two states shown are the H($1s$) entrance channel and the $|7,1\rangle$ protonium channel. As the results of the diabatization, the diabatic channel functions vary smoothly with the hyperradius. At the hyperradius of 60 a.u., the channel functions are well localized around the singularities of the Coulomb potential. This distance is indeed far from the interaction region which occurs for R smaller than about 20 a.u. The H($1s$) channel function presents only one peak, as expected from the ground state. As the hyperradius is decreased to 20 a.u., the channel functions still have similar structures, compared to that of $R=60$ a.u., but extend over a larger region of the angular space. The H($1s$) state remains relatively localized close to $\phi=\pi/2$, but the protonium state moved from small values of ϕ to about $\pi/4$. At $R=15$ a.u., we have entered the interaction region as can be seen from the two channel functions which occupy similar angular space and thus a larger overlap between neighboring points is expected. The overlap between the H($1s$) and Pn($|7,1\rangle$) states was indeed found to be rather large. However, by looking at the other protonium states (not shown here), the overlap of the H($1s$) entrance channel with the higher channels of the $n=7$ protonium manifold was found to decrease rapidly, to become practically zero with the highest channel Pn($|7,7\rangle$). This is the consequence of the large difference in the nodal structures of the channel functions. From this analysis we expect protonium formation to occur mostly to the Pn($|7,1\rangle$) state. Similarly, we found that the lowest state from each manifold for the lower manifolds is the most important one for the protonium formation.

In order to reduce the number of channels included in the calculations, we need a way to identify the dominant channels for the collision process. This can be done by comparing the couplings between different channels. In Fig. 5 we show the largest radial couplings as functions of hyperradius from 0 up to 700 a.u. The radial couplings have been evaluated approximately by using Eq. (4). From the figure we see that the largest couplings occur for protonium states of different manifolds that have the same position in the manifolds. For example, the protonium channel $|7,1\rangle$ is strongly coupled to channels $|8,1\rangle$ and $|6,1\rangle$. Similarly the channel $|7,2\rangle$ couples mostly with channels $|8,2\rangle$ and $|6,2\rangle$. However the coupling between channels $|7,1\rangle$ and $|7,2\rangle$ is very small. These different couplings can be explained by the differences in the nodal structure of these states. These results, together with Fig. 4, suggest that the collision will populate preferably the lowest states of manifolds close to the entrance channel.

Figure 5 also indicates that the radial couplings between similar channels from different manifolds decrease quite slowly with the hyperadius. This means that the distribution of the population in the different protonium states can change up to large distances. In practical calculations we did the matching at $R=600$ a.u., and checked the stability of the results against matchings at 500 a.u. and 700 a.u. The slower convergence of the calculation for the present system in comparison to the typical ion-atom collisions is in part due to the mass scaled hyperspherical coordinates used. For ρ_2 greater than ρ_1, the hyperradius is roughly the square root of the reduced mass of μ_2 multiplied by ρ_2. Thus a matching at about 700 a.u. would amounts to a matching at ρ_2 at about 100 a.u. which is not large considering that we are dealing with low-energy collisions. The larger matching radius does not cause any numerical difficulty since the matrix elements are very smooth in the large R region and large step size can be used for the integration.

Table I illustrates our numerical results for the $\bar{p}$-H cross sections at low energies. These cross sections correspond to a total orbital angular momentum $J=0$ (spin is not considered). We have observed that the $J=1$ contribution becomes negli-

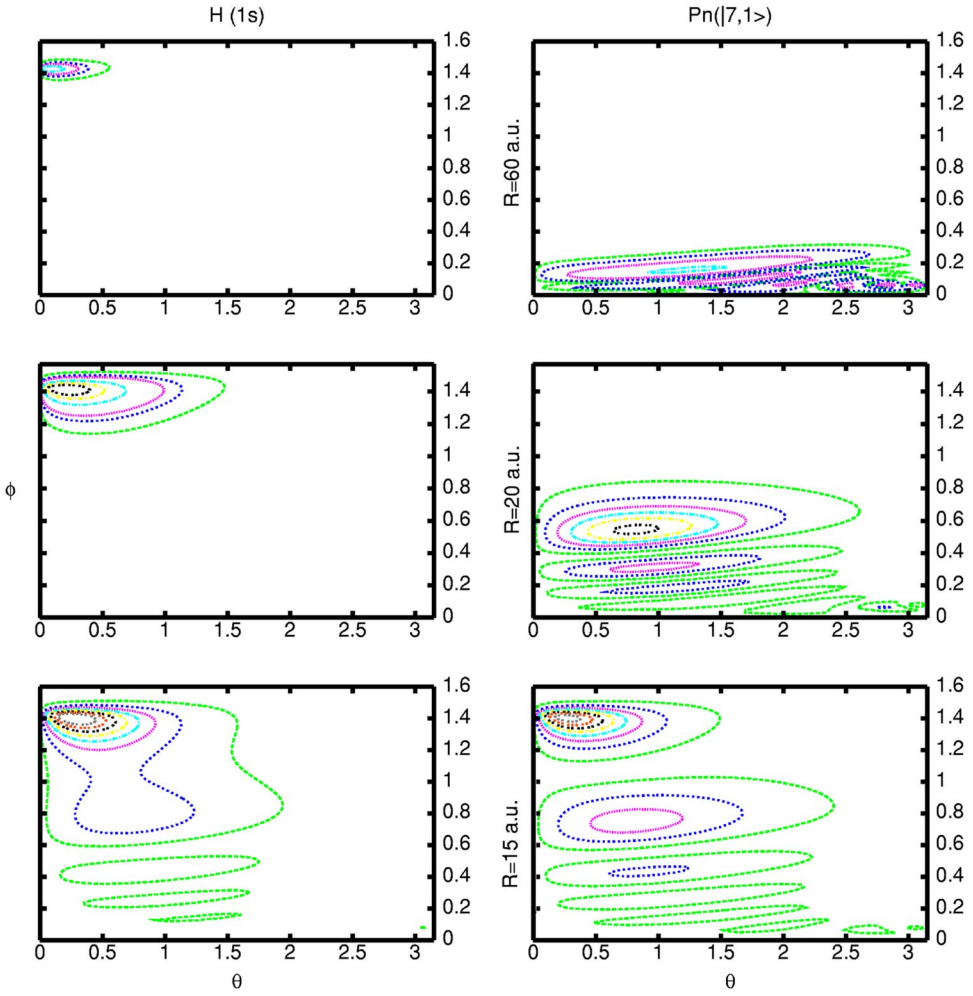

FIG. 4. (Color online) Evolution of the H(1*s*) and Pn($|7,1\rangle$) diabatic channel functions with respect to hyperradius.

gible for antiproton kinetic energies lower than 0.1 a.u. The full HSCC calculation includes 46 channels, i.e., all the protonium states from $n=1$ up to $n=9$. The cross sections are given at five antiproton kinetic energies from about 0.2 a.u. down to 2×10^{-5} a.u. These energies are also indicated in degrees kelvin in order to relate them to the typical energies

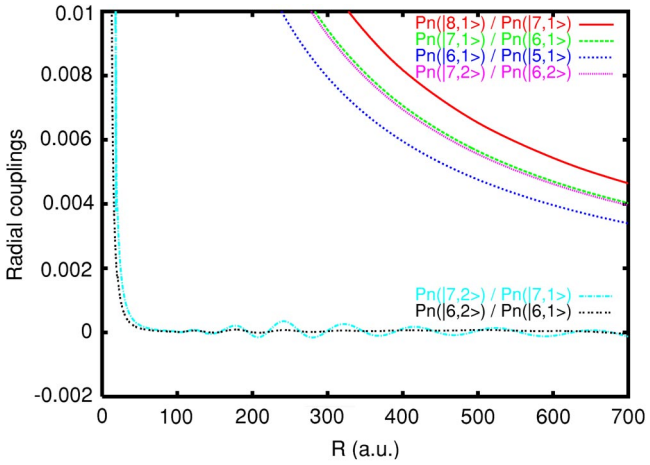

FIG. 5. (Color online) Radial couplings between some protonium channels as functions of hyperradius.

TABLE I. Protonium formation and elastic cross sections (in atomic units), at five antiproton kinetic energies, for a total angular momentum $J=0$. The cross sections correspond to a HSCC calculation including 46 adiabatic channels. The energies are also given in degrees kelvin. The number in square brackets denotes the power of 10.

$E_{\bar{p}}$(a.u.)	1.9 [−1]	3.0 [−2]	2.0 [−3]	3.0 [−4]	2.0 [−5]
$E_{\bar{p}}$(K)	59700	9460	660	94	6.3
$n=1$	8[−8]	6[−7]	1[−5]	1[−4]	1[−3]
$n=2$	3[−6]	1[−5]	7[−4]	4[−3]	0.04
$n=3$	5[−5]	2[−4]	3[−3]	0.02	0.21
$n=4$	5[−4]	2[−3]	0.04	0.29	2.88
$n=5$	0.01	0.03	0.53	3.93	39.9
$n=6$	0.04	0.29	4.11	33.8	354
$\|6,1\rangle$	0.036	0.27	3.79	31.8	333
$\|6,2\rangle$	0.004	0.02	0.31	2.0	20.7
$n=7$	0.11	1.14	16.7	121	1237
$\|7,1\rangle$	0.11	1.12	16.4	118	1212
$\|7,2\rangle$	0.00	0.01	0.27	2.15	22.2
Total	0.16	1.46	21.4	159	1634
Elastic	0.47	0.53	7.04	464	1703

TABLE II. Comparison of $J=0$ cross sections for the $\bar{p}$-H collision obtained by the 46 adiabatic channels calculation (see Table I) and the truncated one including only 10 diabatic channels. The number in square brackets denotes the power of 10.

	46 channels	10 channels	46 channels	10 channels
$E_{\bar{p}}$ (a.u.)	3.0 [−2]	3.0 [−2]	3.0 [−4]	3.0 [−4]
$E_{\bar{p}}$ (K)	9460	9460	94	94
$\|4,1\rangle$	2[−3]	8[−4]	0.29	0.08
$\|5,1\rangle$	0.03	0.02	3.93	2.04
$n=6$	0.29	0.33	33.8	32.7
$\|6,1\rangle$	0.27	0.30	31.8	29.9
$\|6,2\rangle$	0.02	0.03	2.0	2.78
$n=7$	1.14	1.12	121	123
$\|7,1\rangle$	1.12	1.12	118	120
$\|7,2\rangle$	0.01	0.02	2.15	2.68
Total	1.46	1.47	159	158
Elastic	0.53	0.55	464	467

in a trap (a few degrees kelvin). The table contains the total protonium formation cross sections to the manifolds $n=1$ to $n=7$, and to the lowest states of the $n=6$ and 7 manifolds. The tabulated results show two trends. First, the protonium formation cross sections increase rapidly with decreasing energy. Indeed, the total protonium formation cross section goes from about 0.2 a.u. at the energy of 0.2 a.u. up to about 1600 a.u. at the energy of 2×10^{-5} a.u. Secondly, the protonium formation cross sections drop drastically as the channel index decreases from $n=7$ (dominant) down to the $n=1$. Also, the formation occurs mostly to the lowest states of each manifold. This is in agreement with the analysis of diabatic potential curves and radial couplings.

From the results of Table I, we can now consider the elimination of weak channels in order to reduce the size of the calculations. As explained before the choice of the channels included in the calculations is based on the analysis of couplings. In Table II we present a comparison of cross sections obtained by the full calculation, i.e., including 46 channels, and a truncated calculation including only 10 channels. According to the previous results, the 10 channels are chosen as the lowest states of the different manifolds. More precisely, we choose the lowest state of manifold $n=3$ to $n=8$, and the second lowest state of manifolds $n=6,7$ and 8. The tenth channel is the H(1s) entrance channel. The most important diabatic potential curves for this calculation are illustrated in Fig. 6. They correspond to the two lowest protonium states of manifolds $n=6,7$ and 8, and to the H(1s) entrance channel. Figure 6 shows clearly the broad avoided crossing between the H(1s) entrance channel and the Pn($|7,1\rangle$) protonium state.

Table II compares the cross sections of the two calculations at two kinetic energies of the antiproton. The results of the truncated calculation are in very good agreement with the full calculation. The error due to the elimination of channels is indeed less than a few percents for the dominant channels. The formation cross sections to the lowest states, such as

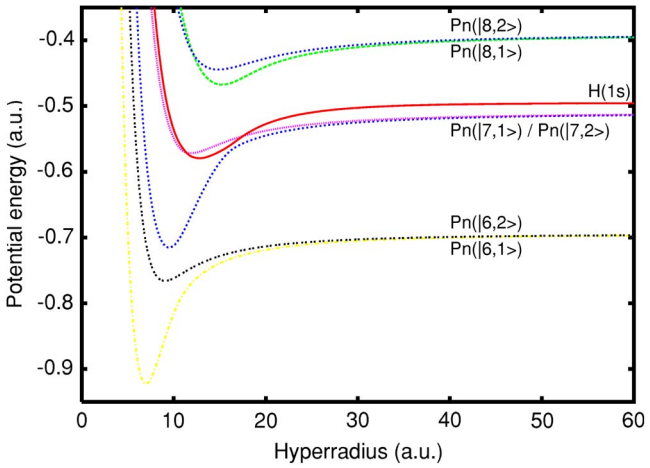

FIG. 6. (Color online) Main hyperspherical diabatic potential curves for $\bar{p}$-H included in the 10-channel calculation. The 6 channels which dissociate to the two lowest protonium states of manifolds $n=6,7$ and 8 are shown together with the H(1s) entrance channel.

$|4,1\rangle$ and $|5,1\rangle$ channels, are not as good. In any event, this is not important as the cross sections for these states are very small in comparison with the dominant states of $n=6$ and $n=7$. Even the elastic cross section is well reproduced with only 10 channels. These results show clearly that weak channels can be removed from the calculation without significant loss of accuracy of the cross sections at low energies.

In Fig. 7 we show the main protonium formation cross sections times the velocity (a measure of the rate constant), obtained by the 10-channel calculation, with respect to the antiproton kinetic energy down to very low energies. The total protonium formation and elastic cross sections are also plotted. Note that a rate constant of 1 a.u. corresponds to 6.13×10^{-9} cm^3/s. This figure illustrates the fast increase of the protonium formation rate with decreasing energy. The total protonium formation cross section is about 10000 a.u. at an energy of 10^{-6} a.u. At very low energies these cross sections display the expected behavior according to the

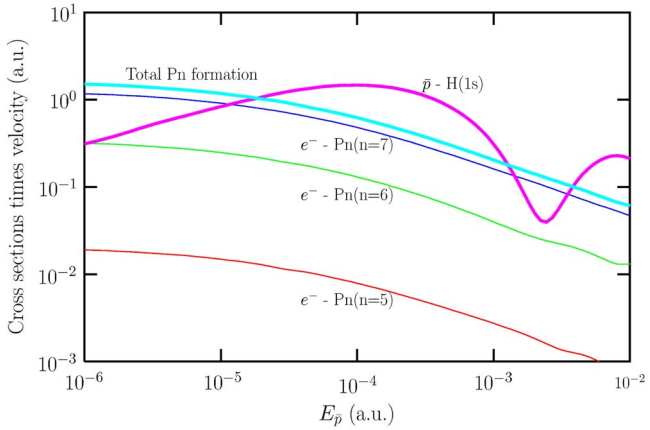

FIG. 7. (Color online) Protonium formation cross sections time the velocity obtained by a 10-channel calculation, as functions of the antiproton kinetic energy. The total protonium formation and elastic cross sections are also shown.

Wigner threshold law [28]. The elastic cross section tends to a constant value, and the total protonium formation cross section behaves like $1/v$, i.e., the formation rate tends to a constant value.

IV. SUMMARY AND CONCLUSIONS

In this paper we have combined the hyperspherical close-coupling method with a diabatization technique which transforms sharp avoided crossings in potential curves into real crossings. With this approach, we have investigated the elimination of weak collision channels from the close-coupling calculations.

We have applied this method to the study of the $\bar{p}$-H collision at low energies. In order to simplify the problem, we have considered a model system where the (anti)proton mass is chosen to be 100 a.u. instead of the real value of 1837 a.u. Our results are consistent with the previous study of Esry and Sadeghpour [15] where the mass of the proton and antiproton were taken to be less than 20 a.u. In our model study with (anti)proton mass equal to 100 a.u., the dominant protonium formation is to the $n=7$ manifold. We have shown that protonium formation occurs mostly to the lowest states of the different manifolds. With the elimination procedure, we show that only 10 channels are needed to get the cross sections with a few percent error over a broad range at low energies.

These results are encouraging for the treatment of the realistic antiproton-hydrogen collision, with (anti)proton mass of 1837 a.u. The muonic system, which corresponds to an intermediate case with a "proton" mass of 200 a.u., could also be calculated. In that last case, the formation would occur mainly to the $n=10$ manifold. The method introduced in this paper can also be used to study charge transfer reactions in atomic collisions with highly charged ions.

ACKNOWLEDGMENTS

This work was supported in part by Chemical Sciences, Geosciences and Biosciences Division, Office of Basic Energy Sciences, Office of Science, U.S. Department of Energy.

[1] M. Amoretti *et al.*, Nature (London) **419**, 456 (2002).
[2] G. Gabrielse, A. Khabbaz, D. S. Hall, C. Heimann, H. Kalinowsky, and W. Jhe, Phys. Rev. Lett. **82**, 3198 (1999).
[3] G. Gabrielse *et al.*, Phys. Rev. Lett. **89**, 233401 (2002).
[4] V. H. Smith and A. M. Frolov, J. Phys. B **28**, 1357 (1995).
[5] J. S. Cohen, Phys. Rev. A **65**, 052714 (2002).
[6] K. Sakimoto, Phys. Rev. A **66**, 032506 (2002).
[7] J. Révai and V. B. Belyaev, Phys. Rev. A **67**, 032507 (2003).
[8] P. Froelich, S. Jonsell, A. Saenz, B. Zygelman, and A. Dalgarno, Phys. Rev. Lett. **84**, 4577 (2000).
[9] M. Hori *et al.*, Phys. Rev. Lett. **87**, 093401 (2001).
[10] D. R. Schultz and P. S. Krstić, Phys. Rev. A **67**, 022712 (2003).
[11] A. Y. Voronin and J. Carbonell, Phys. Rev. A **57**, 4335 (1998).
[12] J. S. Cohen, Phys. Rev. A **36**, 2024 (1987).
[13] J. S. Cohen and N. T. Padial, Phys. Rev. A **41**, 3460 (1990).
[14] K. Sakimoto, J. Phys. B **34**, 1769 (2001).
[15] B. D. Esry and H. R. Sadeghpour, Phys. Rev. A **67**, 012704 (2003).
[16] C. N. Liu, A. T. Le, T. Morishita, B. D. Esry, and C. D. Lin, Phys. Rev. A **67**, 052705 (2003).
[17] A. T. Le, M. Hesse, T. G. Lee, and C. D. Lin, J. Phys. B **36**, 3281 (2003).
[18] A. T. Le, C. N. Liu, and C. D. Lin, Phys. Rev. A **68**, 012705 (2003).
[19] T. G. Lee, A. T. Le, and C. D. Lin, J. Phys. B **36**, 4081 (2003).
[20] B. H. Bransden and M. R. C. McDowell, *Charge Exchange and the Theory of Ion-Atom Collisions* (Clarendon, Oxford, 1992).
[21] T. H. Heil, S. E. Butler, and A. Dalgarno, Phys. Rev. A **23**, 1100 (1981).
[22] J. Q. Sun and C. D. Lin, J. Phys. B **25**, 1363 (1992).
[23] A. Russek and R. Furlan, Phys. Rev. A **39**, 5034 (1989).
[24] R. Cimiraglia, J. P. Malrieu, M. Persico, and F. Spiegelmann, J. Phys. B **18**, 3073 (1985).
[25] B. D. Esry and H. R. Sadeghpour, Phys. Rev. A **68**, 042706 (2003).
[26] K. Nobusada, O. I. Tolstikhin, and H. Nakamura, J. Phys. Chem. A **102**, 9445 (1998).
[27] O. I. Tolstikhin, S. Watanabe, and M. Matsuzawa, J. Phys. B **29**, L389 (1996).
[28] H. R. Sadeghpour *et al.*, J. Phys. B **33**, R93 (2000).